neous media, in asymmetric focusing or scattering). The resulting effect is known as the Spin Hall effect of light.

- *(c) Interaction between intrinsic OAM and extrinsic OAM*, dealing with intrinsic OAM dependent shift of the beam trajectory. This phenomena is similar to (b) and is observed in similar systems but for higher-order beams (carrying intrinsic OAM), accordingly known as Orbital Hall effect of light. This effect may also be termed as the Orbit-orbit interaction (OOI) of light.

As we discuss below, generation of geometric phases and subsequent conservation of total angular momentum of light is inherent to all the optical SOI phenomena. Before we proceed further on defining geometric phase of light, we just note two important features of geometric phases in the context of SOI of light. First, generation of the azimuthal geometric phase (for spherically or cylindrically symmetric systems) is the origin of the spin-to-orbital angular momentum conversion (and the subsequent generation of spin-induced vortices). When we deal with finite beams (such as the fundamental or higher order Gaussian beams, which have a spread in k vector space), the different k vectors of the beam acquire slightly different geometrical phases. The resulting k-gradient of the geometric phase eventually leads to the polarization (the intrinsic SAM) or the intrinsic OAM dependent shift in the trajectory of the beam (or the center of gravity of the beam). Next, it is this second effect that is analogous to the splitting of the energy levels of doubly degenerated bands for spin-up and spin-down electrons, as a consequence of SOI (the spin-orbit energy in Eq. (12.15). Here, the SOI (or OOI) of light lifts the degeneracy in the spatial modes (spatial distribution) between the opposite circular polarization (intrinsic SAM) or the optical vortex (intrinsic OAM) states. This can also be treated as the dynamical manifestation of geometric phases.

12.3 Geometric phase of light

It is wellknown that the propagation of light is associated with a phase factor that depends upon the optical path length ($\Theta_d = \frac{2\pi}{\lambda} \times$ *optical path*). This phase factor is termed as the 'dynamical phase,' and it is responsible for most of the observable interference effects. The 'geometric phase,' on the other hand (as its name suggests), is independent of the optical pathlength and is determined solely by the geometry, or more specifically by the topology of the evolution of the electromagnetic wave. This phase is intimately connected to the change in the polarization state of the EM wave when it undergoes evolution in an inhomogeneous isotropic/anisotropic medium. There are two types of geometric phase;

- *(i) The spin redirection Berry phase*: This arises from a parallel transport of the wave field under continuous variation of the direction of propagation of the wave. In this case, the wave vector **k** (representing the direction of propagation of the wave) changes smoothly (adiabatically) so that in the local reference frame attached to the wave, the state of polarization of the wave does not change. In this so-called 'adiabatic evolution' of the **k** vector imparted by slowly varying changes in the local environment (e.g., the refractive index gradient in a smoothly inhomogeneous medium), when the wave completes a full cyclic evolution (in the k-space), it acquires an additional phase factor independent of the pathlength. This is manifested as a change in the direction of the polarization (rotation of the polarization vector or the polarization ellipse) of the wave when observed from a global reference frame. This topological phase factor was originally discovered by Berry in the 1980s in context to the quantum interference effect [130, 131]. It was subsequently shown by a series of papers that this phase factor is universal and can be observed for classical polarized light also in its evolution in curved trajectory (set by refractive index variation).

- *(ii) Pancharatnam-Berry phase*: This arises for a wave propagating in a fixed direction (fixed k-vector) but undergoing a continuous change in the state of polarization while propagating through an anisotropic (birefringent) medium [131]. When the wave completes a full cyclic evolution in the polarization state space (closed loop in the Poincaré sphere, defined in the Section 6.1.5 of Chapter 6), it acquires an additional geometrical phase factor. This geometric phase related to the continuous and cyclic evolution of the polarization state of light was originally discovered by Pancharatnam in the 1950s.

In the following section, we briefly address the origin of the geometric phase factors and their manifestations, with selected examples.

12.3.1 Spin redirection Berry phase

As noted before, this type of the geometric phase is associated with the adiabatic evolution of the wave vector **k**, when the wave propagates in a curved trajectory set by the spatial variation of the local optical parameters (refractive index) [126, 128]. A convenient example of this is the propagation of the polarized wave in a helically wound circular wave guide (optical fiber, shown in Fig. 12.3(a)). The condition for perfect adiabatic evolution requires (a) that there be no sharp kink (in the scale of wavelength) in the fiber so that the helicity of the wave (handedness of the circular/elliptical polarization) does not change locally as it propagates, and (b) that the medium have no birefringence (anisotropy) effect that can cause local changes in the state of polarization of light. In the example shown in Fig. 12.3(a), the laboratory coordinate frame is

represented by Cartesian coordinates (X, Y, Z) and the local coordinate frame attached to the ray is shown by (v, w, t). The corresponding direction of the polarization vector is denoted by the vector $\mathbf{e}$. In the general case of elliptically polarized light, the direction of $\mathbf{e}$ corresponds to the orientation of the major axis of the ellipse. As is apparent from the Fig. 12.3(a), when the wave propagates through the helical waveguide, the local coordinate frame (v, w, t) undergoes continuous rotation; so does the polarization vector $\mathbf{e}$. Therefore, in the local coordinate frame attached with the ray, the polarization does not change. It is convenient to represent such adiabatic evolution processes of polarized waves in the momentum space (k-space), where the direction of propagation of the wave is represented by the three Cartesian components of the wave vector (k_x, k_y, k_z) in the k-sphere (which is the parameter space here with k_x, k_y, k_z as the three axes, shown in Fig. 12.3(b)). The spherical angles of the k-sphere are represented as (θ, ϕ), and accordingly the direction of the wave momentum with respect to the laboratory coordinate frame (X, Y, Z) can be represented as

$$(k_x, k_y, k_z) = k(\sin\theta\cos\phi, \sin\theta\sin\phi, \cos\theta). \tag{12.16}$$

Note that θ is the angle between the local waveguide axis and the axis of the helix (Z-axis) (i.e., the pitch angle of the helix) and ϕ is the azimuthal angle related to the winding of the helix (one full winding period corresponds to $\phi = 2\pi$). One full cyclic evolution of the k-vector (closed loop at the k-sphere) corresponds to one period of the trajectory of the helically wound optical fiber. As apparent from Fig. 12.3(a), in one full cyclic evolution, although the polarization vector $\mathbf{e}$ (orientation of the polarization ellipse) never changes its direction in the local frame (attached to the ray), in the global laboratory frame (X, Y, Z), it is rotated by an angle Θ. The corresponding closed loop at the k-sphere is shown in Fig. 12.3(b). The surface spanned over the closed loop is observed to subtend a sold angle (area enclosed by the projection of the loop onto the k-sphere) at the center of the sphere, which is exactly equal to Θ. This solid angle can be calculated as

$$\Theta = \int_0^{\theta} \sin\theta d\theta \int_0^{2\pi} d\phi = 2\pi(1 - \cos\theta). \tag{12.17}$$

Let's now try to interpret the observed rotation of the polarization in terms of the geometric phase of light. For simplicity, we assume that the input light is linearly polarized, in principle; this can also be generalized for any arbitrary elliptically polarized wave. The rotation Θ of the linear polarization vector due to one full cyclic evolution of the wave in the helical waveguide can be interpreted as an 'optical rotation' effect. As we have seen in Chapter 6 (Section 6.2.3), that optical rotation is a manifestation of the circular birefringence effect (which arises from a phase difference between orthogonal circular polarization states). However, the waveguide has no local intrinsic anisotropies or circular birefringence. The observed circular birefringence thus appears to

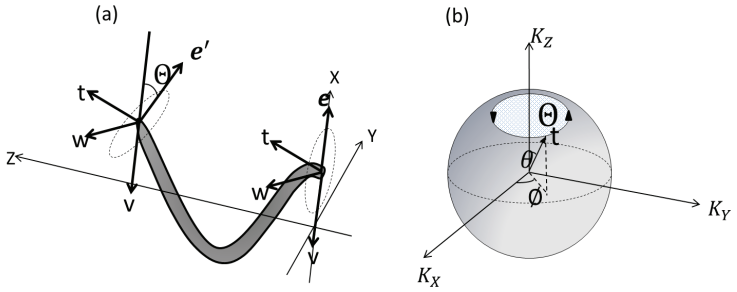

FIGURE 12.3: (a) Propagation of polarized light in a helical wound circular waveguide (optical fiber). The laboratory reference frame is represented by (X, Y, Z) Cartesian coordinates, the local reference frame attached to the ray is shown by (v, w, t), and the corresponding direction of the polarization vector (or orientation of the polarization ellipse) is denoted by the vector **e**. One full cyclic evolution of the polarized wave leads to a rotation of the polarization vector by an angle Θ. (b) Representation of one full cyclic evolution in the momentum space (wave vector k- space). The spherical angles of the k-sphere are represented as (θ, ϕ); θ is the angle between the local waveguide axis and the axis of the helix (z-axis) (the pitch angle of the helix) and ϕ is the azimuthal angle. The closed loop at the k-sphere corresponding to one full cyclic evolution subtends a solid angle Θ at the center of the sphere.

be a geometrical effect. This can be understood in a simple way if we consider linearly polarized light to be superposition of equal amplitude of left (L) and right (R) circular polarization. We may write the input linear polarization state (say, oriented along x-axis of the laboratory coordinate) as

$$|x\rangle = \frac{1}{\sqrt{2}} \left(|L\rangle + |R\rangle \right). \tag{12.18}$$

The state of linear polarization of the wave after one fully cyclic evolution (rotated by an angle Θ) is given by

$$|x_{out}\rangle = \frac{1}{\sqrt{2}} \left(\exp(i\Theta)|L\rangle + \exp(-i\Theta)|R\rangle \right). \tag{12.19}$$

It appears from Eq. (12.19) that while propagating through the helical waveguide, the constituent left and right circular polarization modes of the linearly polarized wave have acquired equal and opposite phases ($\pm\Theta$), which does not originate from any intrinsic anisotropies and is thus purely geometric in nature. This is the so-called spin redirection Berry phase. As is apparent from Eq. (12.17), for one full cyclic evolution (due to continuous change in the trajectory of the polarized light wave), the spin redirection Berry phase is

determined by the solid angle subtended by the closed loop in the k-sphere (in the momentum domain representation).

The spin redirection Berry phase may also be directly measured in the following interference experiment. A circularly polarized (either left or right) laser beam is coupled to an optical fiber, which in turn couples equal amount of light into two helically wound optical fibers. Each of these fibers have N number of turns but in the opposite sense (right and left helix), which are adjusted to have equal optical pathlengths. These two oppositely wound helical fibers constitute the two arms of the interferometer. The fibers are then once again brought together and coupled to another single output optical fiber. The interference is observed at the output optical fiber using a detector. As apparent from Eq. (12.17), circularly polarized light while propagating through the two arms acquire equal and opposite amount of geometric phases ($\Theta = \pm 2\pi N(1 - \cos\theta)$) (the factor N arises due to N number of cyclic evolutions). The resultant intensity pattern would therefore be

$$I = I_0 \cos^2[2\pi N(1 - \cos\theta)]. \tag{12.20}$$

The resultant output intensity after the interference would thus be determined by the pitch angle of the helix (θ) and the number of turns N.

12.3.2 Pancharatnam-Berry phase

The Pancharatnam-Berry phase arises when a polarized wave undergoes continuous change in the state of polarization, keeping the direction of propagation fixed (fixed k-vector). An additional geometrical phase factor is introduced when the wave completes a full cyclic evolution in the polarization state space (in the Poincaré sphere) [131, 132, 133]. Clearly, such a situation may arise when polarized light propagates through homogeneous/inhomogeneous anisotropic (birefringent) medium. In order to illustrate this, in Fig. 12.4(a) we show a Michelson interferometer arrangement for observing Pancharatnam phase [133].

Consider linearly polarized (say, a polarization axis oriented along the x-axis of the laboratory coordinate) light from a laser is divided into two equal beams by a 45°, 50: 50 beam splitter. Beam 1 travels to a perpendicular mirror M_1 and is reflected back. Beam 2 first travels through a quarter waveplate $QP1$, whose optical axis is fixed at ($\theta_1 = \pi/4$) relative to the incident x-polarization. This converts the linearly polarized light into right circularly polarized, which then passes through another quarter waveplate, $QP2$, whose optical axis makes and angle $\theta_2 = \left(\frac{3\pi}{4} + \beta\right)$ with the x-axis. The light emerging from $QP2$ strikes perpendicular mirror $M2$, from which it is reflected and made to retrace its path. The beam splitter BS combines portions of the returning light from arms 1 and 2 and gives rise to an interference pattern in arm 3 that allows the phase difference between the two return beams to be determined. In this system, the presence of geometrical phase can be inferred by keeping the lengths of the two arms fixed (thus keeping the dynamical phase

difference fixed between two arms) and by changing the orientation angle θ_2 of the second quarter waveplate $QP2$. Changes in geometrical phase associated with polarization evolution in arm 2 of the interferometer will be manifested as shift of the interference phase (fringe shifts). In order to understand

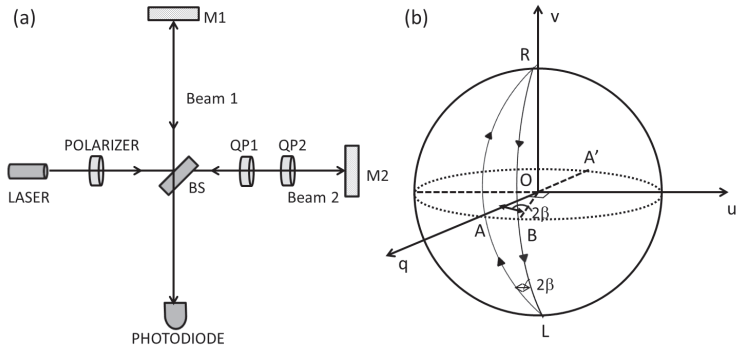

FIGURE 12.4: (a) Schematic of the Michelson interference experiment for observation of Pancharatnam-Berry phase. (b) The evolution of the state of polarization of light in arm 2 of the Michelson interferometer (Fig. 12.4(a)) is shown in the Poincaré sphere (shown for incident x-polarized light). Equatorial points A and A' represent x and y linear polarization, the polar points R and L represent right and left circular polarization. The action of QP1 and QP2 are shown by trajectories AR and RB. After reflection, the polarization state evolves in similar manner but in the opposite sense, represented by trajectories BL and LA. The closed loop corresponding to full cyclic evolution of polarization state (ARBLA) subtends a solid angle 4β, and the corresponding geometric phase is half of this solid angle (2β).

the Pancharatnam-Berry phase resulting from polarization transformations in arm 2 of the interferometer, we model each of the polarizing interactions using Jones matrices (following Section 6.2.3 of Chapter 6). The first quarter waveplate (oriented at $\pi/4$ with respect to the x-axis) transforms the incident x-polarized light (represented by Jones vector $\left[\begin{array}{cc} 1 & 0 \end{array}\right]^T$) into a right circularly polarized (RCP) light

$$\left[\begin{array}{cc} 1+i & 1-i \\ 1-i & 1+i \end{array}\right]\left[\begin{array}{c} 1 \\ 0 \end{array}\right] = \left[\begin{array}{c} 1 \\ -i \end{array}\right]\exp(i\phi_1). \tag{12.21}$$

Here, we have used the Jones matrix of a quarter waveplate oriented at an angle $\pi/4$ (orientation angle $\theta_1 = \pi/4$, retardance $\delta = \pi/2$ in Eq. (6.37). As is apparent from Eq. (6.37), the phase factor ϕ_1 here is related to the thickness and refractive index of the birefringent waveplate and is therefore a dynamic

one. The resulting RCP light passes through the second quarter waveplate (QWP2 oriented at $\theta_2 = \left(\frac{3\pi}{4} + \beta\right)$)) to yield linearly polarized light

$$\begin{bmatrix} \cos^2\theta_2 + i\sin^2\theta_2 & (i-1)\sin\theta_2\cos\theta_2 \\ (i-1)\sin\theta_2\cos\theta_2 & \sin^2\theta_2 + i\cos^2\theta_2 \end{bmatrix} \begin{bmatrix} 1 \\ -i \end{bmatrix} = \begin{bmatrix} \cos\beta \\ \sin\beta \end{bmatrix} e^{(i\phi_2)} \times e^{(-i\beta)}. \tag{12.22}$$

It is important to note that the polarized light acquires an additional phase factor $\exp(-i\beta)$ depending upon the orientation angle (θ_2 is related to β with a constant factor) of the waveplate in addition to the dynamical phase factors (ϕ_1 and ϕ_2). The linearly polarized light then gets reflected from the mirror and undergoes similar evolution through the two quarter waveplates. The action of QP2 (which is now oriented at an angle $\pi/4$ with respect to the direction of linear polarization of the reflected wave) will convert the linearly polarized light into a left circularly polarized light (LCP, when represented in the same reference frame) and will introduce another phase factor $\exp(-i\beta)$ in addition to the dynamical phase factor. Finally, when the LCP light passes through QP1, it will be converted back to x-polarized light $\begin{bmatrix} 1 & 0 \end{bmatrix}^T$. Thus, in this process, the input x-polarized wave completes a full cyclic evolution in the polarization state space. During this evolution, it acquires a total dynamic phase

$$\phi_d = 4 \times \frac{2\pi}{\lambda} \times \frac{(n_e + n_o)}{2} d, \tag{12.23}$$

where n_e and n_o are the refractive indices of the slow and fast components in the quarter waveplates and d is the thickness of the waveplate so that the retardance $\delta = \frac{2\pi}{\lambda}(n_e - n_o)d = \frac{\pi}{2}$. Importantly, in addition to this dynamical phase, the polarized wave acquires a geometric phase factor $\exp(-2i\beta)$ (geometric phase of 2β), which is independent of the optical pathlength and is only determined by the orientation angle of the second quarter waveplate (thus it depends upon how the polarization state has evolved during the cyclic process).

The evolution of the geometric phase can be conveniently represented by the polarization transformations in the Poincaré sphere (defined in Section 6.1.5 of Chapter 6). The trajectory of the polarization evolution for this particular experimental configuration is shown in Fig. 12.4(b). The four basic interactions in arm 2 of the interferometer can be represented by the following transformations in Poincaré sphere:

1. The incident x-polarized light (noted by position A in the equator region of the sphere) transforms to RCP light (represented by point R in the north pole) by passing through QP1 (trajectory shown by AR).

2. The action of QP2 brings back the state to linear polarization, represented by point B in the equator region (trajectory RB). After reflecting back from the mirror, the polarization state evolves in a similar manner but in the opposite sense.

3. The action of QP2 on the polarization state of the reflected light takes it to L in the south pole (LCP).

4. QP1 then brings the state of polarization to the initial linear polarization (A, representing x-polarization).

Thus the state of polarization performs a closed loop in the Poincaré sphere. As shown by the geometry of the Poincaré sphere in Fig. 12.4(b) (and corresponding analogy of the k-sphere shown in Fig. 12.3(b) for the case of spin redirection Berry phase), the solid angle subtended by this closed loop (ARBLA) at the center of the sphere is given by 4β. The corresponding geometric phase will be half of this solid angle and will thus be equal to 2β. The origin of this $\frac{1}{2}$ factor in the case of Poincaré sphere representation (as compared to the k-sphere) can be understood by noting that the rotation of the polarization ellipse (or polarization vector) by an angle ϕ in the real space corresponds to 2ϕ rotation in the Poincaré sphere (see Eq. (6.46) and subsequent discussion in Chapter 6). We note here that the closed loop shown in Fig. 12.4(b) is for input x-polarized light. In the case of input y-polarized light, the evolution would also be cyclic but given by the reflection of the loop through the origin. The two loops are traversed in opposite senses, and hence they subtend at equal and opposite solid angles at the origin. Thus, input x- and y-polarizations would acquire Pancharatnam-Berry phase of $\mp 2\beta$.

We now briefly touch upon an interesting effect associated with dynamical manifestation of Pancharatnam-Berry phase in context to polarization evolution in anisotropic medium. We now consider the same experiment as above, however, in our experiment the second quarter waveplate (QP2) is uniformly rotated with an angular velocity $\Omega = \frac{d\theta_2}{dt}$. The segment RAL (of the closed loop ARBLA shown in Fig. 12.4(b)) remains unchanged under this rotation, whereas the segment RBL continuously rotates about the axis RL with angular velocity of 2Ω. This will make the geometric phase to evolve with time as $\beta(t) = \beta(0) \mp 2\Omega t$, where the $\mp$ signs are for input x- and y- polarizations, respectively. This linear time variation of the geometric phase therefore contributes to a shift in the frequency. If the input light has a frequency ω, the frequency of the output light (after making the round trip) would become $\omega' = \omega \pm 2\Omega$, for input x- (plus) and y- (minus) polarizations, respectively. Note that the plus or minus signs in the frequency shift is relative and depends upon the convention (how the positive or negative phases are defined). It is also important to note that this effect may also be observed with a single rotating half-waveplate (whose retardation is given by $\delta = \frac{2\pi}{\lambda}(n_e - n_o)d = \pi$). The half-waveplate transforms input RCP light to LCP light ($\sigma = -1 \rightarrow +1$), and the corresponding evolution of the polarization state in the half-waveplate can be represented in Poincaré sphere as shown in Fig. 12.5(a). Note, we may reach to LCP (south pole) from RCP (north pole) using different paths on the sphere, which is determined by the orientation angle of the waveplate (θ) with respect to the laboratory polarization axis (say, the x-axis). The difference in geometric phases between two such paths is half of the solid angle enclosed

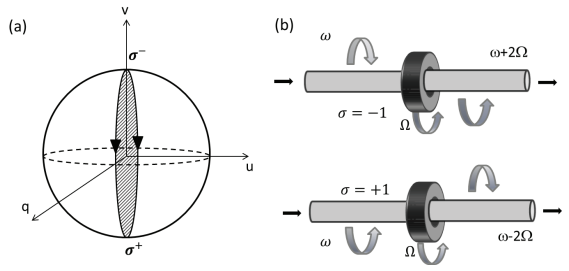

FIGURE 12.5: Dynamical manifestation of the Pancharatnam-Berry phase for a rotating half-waveplate. (a) The half-waveplate converts incident RCP light to LCP light ($\sigma = -1 \rightarrow +1$). The trajectory depends upon the orientation angle of the optical axis of the waveplate with respect to the laboratory axis (say, the x-axis). Two different trajectories corresponding to two orientations (at two different instances) of the rotating waveplate are shown. The difference in geometric phases between two such paths is half of the solid angle enclosed by the loop formed by these two trajectories, shown by the shaded region. (b) The evolving geometrical phase leads to equal and opposite shifts in the frequency for input right and left circularly polarized light. Here, Ω is the angular velocity of the rotating waveplate.

by the loop formed by these two trajectories (shown by the shaded region in the Fig. 12.5(a)). If the waveplate is rotated with uniform angular velocity $\Omega = \frac{d\theta}{dt}$, akin to the previous case, the geometric phase would evolve with time as $\approx \mp 2\Omega t$. However, unlike the previous case, here $\mp$ signs are for input right and left circular polarizations, respectively. This would accordingly lead to a shift of the frequency of the input wave $\omega' = \omega \pm 2\Omega$, for input right (plus) and left (minus) polarizations, respectively. This is the so-called rotational Doppler shift for the SAM-carrying light beam (displayed in Fig. 12.5(b)). As we shall discuss later (in context to the spin-orbit interaction of light in inhomogeneous anisotropic medium), this effect is closely related to SOI and the polarization-dependent shift in the trajectory of a beam (or the center of gravity of a beam).

12.3.3 Geometric phase associated with mode transformation

The geometric phases discussed earlier (spin redirection Berry phase and Pancharatnam-Berry phase) are associated with the polarization state of light (or SAM). From a conceptual point of view, it is expected that analogous geometric phases should also be observed for beam-carrying intrinsic OAM (where the role of SAM is played by intrinsic OAM) [128]. As we now know

that the intrinsic OAM of light is associated with the mode structure of a light beam (transverse distribution of the field amplitude and phase), mode transformation should also lead to the generation of both the variants of the geometric phase. One deals with the geometry of the path in the configuration space (continuous variation of the direction of propagation of the wave and the wave vector k, like the helical trajectory described earlier), leading to a change in the global orientation of the mode structure of the beam. Waves propagate in a fixed direction (fixed k-vector) but undergo a continuous mode transformation (the geometry of the path can be represented in the mode space as was done in the polarization state space for SAM-carrying beams). This can be understood from the following analogy of SAM and OAM [134]. As we have

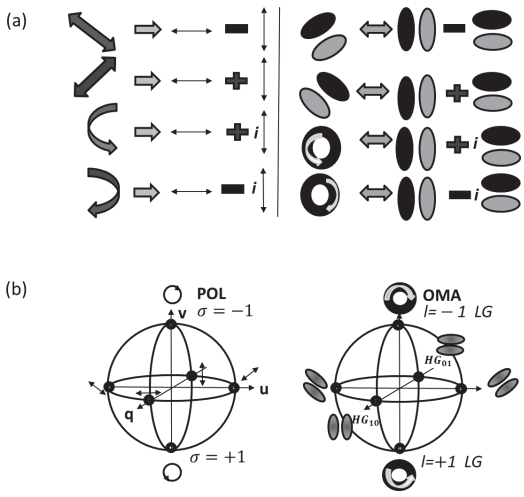

FIGURE 12.6: (a) Decomposition of the polarization states ($\pm 45°$ linear and left/right circular polarizations) using the horizontal and vertical linear polarization basis states (left panel). The corresponding decomposition of $\pm 45°$ oriented HG modes and the left- and right- handed LG modes ($l = \pm 1$) using the HG_{10} and HG_{01} modes. Note that the orientation of the lobes in an HG mode correspond to the direction of linear polarization vector (e.g., HG_{10} horizontal orientation of the lobes $\rightarrow$ horizontal linear polarization). (b) Analogy between the polarization Poincaré sphere (left panel) and orbital Poincaré sphere of first-order modes (right panel). Linear and circular polarization states are shown in the polarization Poincaré sphere, while their analogous HG and LG modes are shown in the orbital Poincaré sphere.

previously discussed, the Laguerre-Gaussian (LG) laser modes have a helical phase front characterized by transverse field distribution $\approx \exp(il\phi)$ (where ϕ is azimuthal angle) and accordingly carry OAM. In fact, the LG modes follow

from the solutions to the paraxial wave equation in cylindrical coordinates, and a general LG mode (LG_p^l) is characterized by radial and azimuthal indices p and l, respectively, carrying $l\hbar$ OAM per photon. The Hermite-Gauss (HG) modes, on the other hand, are solutions to the paraxial wave equation in rectangular coordinates (represented by HG_{nm}) and do not carry OAM as such. The order of these modes is generally given by $N = 2p + |l| = n + m$. We note that for mode with order $N = 1$, in phase superposition of left-handed ($l = +1, p = 0$) and right-handed ($l = -1, p = 0$) helical LG modes form an HG mode with indices $m = 1, n = 0 (HG_{10})$. Similarly, the HG_{01} mode can be obtained by superposition of left and right LG modes with a phase difference of π between them;

$$HG_{10} = LG_0^{+1} + LG_0^{-1} \quad HG_{01} = LG_0^{+1} - LG_0^{-1}. \tag{12.24}$$

Conversely, the first order LG modes may also be obtained by superposition of orthogonal HG modes

$$LG_0^{+1} = HG_{10} + iHG_{01} \quad LG_0^{-1} = HG_{10} - iHG_{01}. \tag{12.25}$$

This set of equations provides the basis for an analogy between Jones vector representation of linear and circular polarization states and those of the first-order HG and LG modes. If we represent the states of the HG_{10} and HG_{01} modes as $[1, 0]^T$ and $[0, 1]^T$ (the equivalent representation of horizontal and vertical linear polarization states), the corresponding orthogonal LG modes (with $l = \pm 1$) can be represented as $\frac{1}{\sqrt{2}}[1, \pm i]^T$ (equivalent representation of left and right circular polarization). In fact, we can do a decomposition of any arbitrarily oriented HG mode (determined by the orientation of the phase structure and intensity distribution) and LG modes using the basis of the HG_{10} and HG_{01} modes, just like any arbitrarily oriented linear polarization state and circular (elliptical) polarization states can be decomposed using horizontal and vertical linear polarization basis. This yields one-to-one correspondence between the first-order modes with the polarization state of light, as shown in Fig. 12.6(a). The corresponding analogy between the Poincaré sphere representation of the polarization states and the mode states in the sphere of the first-order modes (the orbital Poincaré sphere) is shown in Fig. 12.6(b). In the orbital Poincaré sphere of the first-order modes, the poles correspond to right- and left-handed LG modes ($l = \mp 1$, north and south poles), and the equator region corresponds to HG modes oriented at different angles.

From this analogy it is apparent that both the variant of the geometric phase (spin redirection Berry phase and Pancharatnam-Berry phase) associated with polarization state of light should be manifested in the case of the evolution of mode structure in curved trajectory of a light beam or for continuous mode transformation (a change of the OAM state of the beam). Like in the case of spin redirection Berry phase (Fig. 12.3(a)), let us now consider the propagation of an HG laser mode through a helically wound circular waveguide (shown in Fig. 12.7). Here also, for one full cyclic evolution of the k-vector

(corresponding to one period of the trajectory of the helically wound optical fiber), although mode structure does not change in the local coordinate frame attached with the beam, in the global laboratory frame it is rotated by an angle Θ. The corresponding closed loop at the k-sphere and the solid angle subtended by this at the centre of the k-sphere can also be shown to be equal to Θ (similar to Eq. (12.17)). If we consider the evolution of the HG_{10} mode (as an example), the output rotated (by an angle Θ) mode structure after one full cyclic evolution may also be interpreted as

$$|HG_{out}\rangle = \frac{1}{\sqrt{2}}\left(\exp(i\Theta)|LG_0^{+1}\rangle + \exp(-i\Theta)|LG_0^{-1}\rangle\right). \tag{12.26}$$

Apparently, while propagating through the helical waveguide, the constituent left- ($l = +1$) and right-handed ($l = -1$) LG modes of the HG_{10} mode acquires equal and opposite phases ($\pm\Theta$), which is the geometric phase. In an analogy with polarization, this may be termed as the *OAM redirection Berry phase*. The other variant of the geometric phase arises when the laser beam

FIGURE 12.7: Propagation of a HG laser mode through a helically wound circular wave guide. One full cyclic evolution of the k-vector (corresponding to one period of the trajectory of the helically wound optical fiber) leads to a rotation of the mode structure by an angle Θ.

propagates in a fixed direction (fixed k-vector) but undergoes a continuous mode transformation (the Pancharatnam-Berry equivalent geometric phase for mode transformation). This type of geometric phase can be observed using a Michelson interferometer arrangement similar to that of the Pancharatnam phase associated with polarization transformation (Fig. 12.4(a)). The polarization states of light in this experiment have to be replaced by the corresponding mode states (according to Fig. 12.6(a)). We may start with a HG_{10} mode (in place of the horizontal linear polarization), which is then split into the two arms of the interferometer using a beam splitter. Beam 1 once again

travels to a perpendicular mirror M_1 and is reflected back. Beam 2 undergoes continuous mode transformations in the second arm of the interferometer. As we have previously discussed, when a pair of cylindrical lenses is kept at $2f$ distance away with their focal lines parallel, they act as $\pi/2$ mode converter. The direction of the focal lines of the cylindrical lenses is referred to as the principal axis of the converter. The $\pi/2$ mode converter in the OAM basis plays the role of a quarter waveplate in the SAM basis, and accordingly it can convert Hermite-Gaussian (HG) laser modes into LG modes (carrying OAM) when the principal axis of the converter is kept at angle $\pm 45^\circ$ with respect to the axis of the HG mode. Thus in this experiment, the two quarter waveplates (QP1 and QP2 of Fig. 12.4(a)) may be replaced by two $\pi/2$ mode converters. The orientation of the principal axis of the first mode converter can be fixed at 45°, whereas the orientation of the second mode converter may be changed to observe the resulting geometric phase associated with the mode transformation (which would be manifested in the interferogram). The trajectory of the mode transformation and the evolution of the OAM state here can be represented in the orbital Poincaré sphere of first-order modes (Fig. 12.6(b)) in an exactly similar fashion as that was done for polarization evolution in the polarization Poincaré sphere (Fig. 12.4(b)) (in order to avoid repetition, the corresponding representation in the orbital Poincaré sphere is not shown here). The corresponding geometric phase associated with mode transformation would also be half of the solid angle enclosed by the closed loop in the center of the orbital Poincaré sphere (solid angle=4β and geometric phase=2β, where β is the orientation of the principal axis of the second $\pi/2$ mode converter).

Having described the various types of geometric phases, we are now in a position to discuss spin-orbit interaction of light. In what follows, we describe three specific cases of SOI with illustrative examples; SOI in inhomogeneous anisotropic media, in scattering and in tight focusing of a fundamental Gaussian beam. We shall outline the mathematical framework for describing SOI and discuss the role of geometric phases in the resulting SOI.

12.4 Spin-orbit interaction of light in inhomogeneous anisotropic medium

So far, we have seen that when a polarized light beam propagates through an anisotropic medium (either birefringent or dichroic), its state of polarization changes. This aspect has been dealt within some detail in Chapter 6, where it was discussed that the two of the important anisotropic properties of the medium, linear birefringence (retardance) and linear dichroism (diattenuation) arise from the differences in the real and imaginary parts of the